Compressive Strength Performance of 3D Printed PLA/Almond Shell Particles Reinforced PLA multi-material Composite

P. Saravanamuthukumar [1], J Kaaviya[2] , Sabarinathan Palaniyappan [3, *], Narain Kumar Sivakumar [4], Mahdi Bodaghi[5], Mostafizur Rahaman[6], Saravanan Pandiaraj[7]

[1]*Department of Mechanical Engineering, Amrita college of engineering and technology, Nagercoil, Tamil Nadu, India.* Saravana33mech@gmail.com

[2]*Department of Computer Science and Engineering, Saveetha Engineering College (Autonomous), Saveetha Nagar, Thandalam, Chennai, Tamil Nadu, India – 602105.*

[3] *Centre for Molecular medicine and diagnostics, Saveetha Dental College, Saveetha Institute of Medical and Technical Sciences, Saveetha University, Chennai, Tamil Nadu, India.* sabarinathan14010@mech.ssn.edu.in

[4] *Centre for Molecular medicine and diagnostics, Saveetha Dental College, Saveetha Institute of Medical and Technical Sciences, Saveetha University, Chennai, Tamil Nadu, India.* narainkumars.mech2020@citchennai.net

[5]*Department of Engineering, School of Science and Technology, Nottingham Trent University, Nottingham NG11 8NS, UK;* email: mahdi.bodaghi@ntu.ac.uk

[6]*Department of Chemistry, College of Science, King Saud University, P.O. Box 2455, Riyadh 11451, Saudi Arabia.* mrahaman@ksu.edu.sa

[7]*Department of Self-Development Skills, King Saud University, Riyadh, 11362, Saudi Arabia.* psaravanan.c@ksu.edu.sa

Abstract

The advent of 3D printing has revolutionized the manufacturing landscape, enabling the creation of intricate structures and personalized designs. The use of multi-material polymer composites in additive manufacturing has further expanded possibilities, offering enhanced mechanical properties and advanced functionalities. In the present study, PLA/Almond shell reinforced PLA (PLA/AmdPLA) multi-material composites were developed using Fused Filament Fabrication (FFF) method. The objective of this study is to develop the multi-material and optimize the 3D-Printing Parameters (3D-PP) with respect to Printing Speed (PS), Layer Height (LH), and Printing Temperature (PT), in order to maximize the compressive strength of the composites. The L_{16} Taguchi orthogonal array was established to systematically study the effects of the 3D-PP on the compressive strength. Through a series of experiments, varying the levels of each 3D-PP, data was collected and analyzed to determine the optimal 3D-PP settings. The results demonstrate that the PLA/AmdPLA multi-material composites achieved its maximum compressive strength when fabricated at a PS of 20 mm/sec, a LH of 0.1 mm, and a PT of 210°C. Furthermore, the findings revealed that the PS and LH significantly influenced the compressive strength, while the PT exhibited moderate effects. The regression analysis results indicate that the compression experiments conducted on the PLA/AmdPLA multi-material composites yielded an error percentage of 4.73%. This suggests a strong agreement between the predicted values obtained from the regression model and the actual experimental results which shows that the model has high accuracy.

Therefore, these functional composite materials are recognized for their superior strength, lightweight properties, appealing aesthetics, and sustainable qualities in various consumer applications.

Keywords: Bio-composite; Almond shell; 3D printing; Compression; Optimization.

1. Introduction

In the 1980s, the concept of rapid prototyping emerged, leading to the development of various Additive Manufacturing (AM) technologies. Furthermore, although AM initially focused on prototyping, these technologies have advanced significantly over the past two decades, evolving into sophisticated methods for manufacturing functional parts [1]. Among the various AM techniques, Selective Laser Sintering (SLS) and Fused Deposition Modeling (FDM), also referred to as Fused Filament Fabrication (FFF), are the most widely employed polymer 3D printing methods [2]. FFF offers several advantages over SLS, including lower energy consumption, reduced material costs, minimal waste, and consistent accuracy in prototypes. Additionally, FFF does not require chemical post-processing and utilizes more cost-effective machinery and materials, making it a more economical manufacturing option [3]. The most widely utilized polymeric FFF filaments include PLA (Polylactic acid), ABS (Acrylonitrile butadiene styrene), HIPS (High Impact Polystyrene), PEEK (Polyether ether ketone), TPU (Thermoplastic Polyurethane), etc [4].

Functionally Graded Materials (FGMs) represent an innovative category of composite materials, characterized by a gradual shift in composition and structure across their volume, resulting in specific properties tailored for various regions [5]. Nature offers similar examples of FGMs, such as the diverse trabecular structures in bones and the varied tissue patterns found in seashells and plants like Norway spruce and bamboo [6]. Niino et al. introduced the concept of FGMs for applications in thermal barriers, sparking extensive research in the field [7]. Unlike isotropic bulk materials, FGMs allow for precise control over their composition and structure, facilitating the customization of multifunctional properties [8]. This unique feature has spurred increasing interest in FGMs for applications across aerospace, automotive, nuclear power generation, sensors, biomedical implants, optoelectronic devices, and energy absorption systems [9].

With the progress in AM technologies, the creation of multi-phase materials with gradual composition and structural changes has become feasible, giving rise to Functionally Graded Additive Manufacturing (FGAM) [10]. FGAM entails a layer-by-layer fabrication process, facilitating the incremental modification of material composition within a component's volume [11]. Pioneering research is underway in the development of functionally graded

polymeric materials using the FGAM technique. Several pertinent studies on fabricating FGMs are as follows:

Singh et al. utilized the FDM process to print multi-material (ABS, PLA, HIPS) 3D printed components. The experimental results demonstrated a significant enhancement in the mechanical properties of multi-material 3D printed components compared to the mechanical properties of neat, single-layered individual materials. Additionally, they proposed that placing high-strength ABS as the middle layer and using low-strength PLA as alternating layers at the outer phase of the multi-material results in higher strength [12]. Lopez & Ahmad investigated the mechanical properties of multi-polymer sandwich specimen composed of various materials such as PLA, ABS, and HIPS, fabricated using the FFF process. In the instance of multi-material specimens, the arrangement of materials plays a vital role in enhancing mechanical properties. They reported that, the PLA-ABS-PLA material arrangement exhibited superior mechanical properties compared to other arrangements [13].

Polylactic acid (PLA) is a naturally synthesized polymeric material primarily used as the raw material for the FFF 3D printing process due to its lower production cost, biodegradability, and adaptability [14]. However, one of the main drawbacks of PLA polymer is its brittleness and lower impact strength. To enhance the ductility of the PLA polymer, various reinforcements are added to the PLA matrix. Among these reinforcements, naturally available wood-based reinforcements offer significant advantages such as low cost, biodegradability, and better recyclability [15].

Prunus Amygdalus L., commonly known as almond, is a globally cultivated crop highly valued for its almond shell. Major producers of Prunus Amygdalus are located in Gulf countries, covering approximately 1.7 million hectares of land and yielding around 2.31 metric tons per year in 2017 [16]. A significant byproduct of Prunus Amygdalus cultivation is almond residue, which remains after extracting the almond seed. Unfortunately, this residue is often disregarded and considered suitable for incineration. The husk component, a byproduct of removing the almond seed from the fruit, is typically treated as waste despite containing a substantial amount of cellulose, constituting about 31% of its composition [17].

Furthermore, with the addition of naturally derived reinforcements, various studies are available on the composite filament extrusion of polymeric 3D printing processes. Huda et al. discovered that PLA reinforced with maple wood exhibited better strength than pure PLA. PLA/wood materials hold potential for use in fabricating FFF parts due to the strong adhesion between wood flour and PLA [18]. However, there are limited studies available on the development of multi-materials from novel wood-reinforced PLA composites. Sabarinathan et

al. developed a multi-material PLA composite using walnut shell as reinforcement. They experimented with various stacking sequences to create the multi-material composite. The results clearly indicate that the 50:50 stacking sequence demonstrates superior mechanical and thermal properties [19].

In the pursuit of developing Single Gradient Functionally Graded Materials (SGFGM) using novel extruded composite filaments, it is crucial to consider the 3D-Printing Parameters (3D-PP) to improve the mechanical characteristics of the composite. Ongoing research aims to optimize 3D-PP for organic particle-added composites, as evidenced by the following studies:

Ayrilmis et al. assessed the influence of Layer Height (LH) on the mechanical properties of PLA/wood 3D printed composites. They concluded that smaller LH resulted in superior mechanical properties compared to higher layer thickness [20]. Chohan et al. studied the influence of 3D-PP of the FFF technique, including LH, orientation angle, raster angle, raster width, and air gap on various mechanical characteristics. The experimental results revealed that a layer thickness of 0.127 mm resulted better results for both impact and tensile strength [21]. Vanaei et al. examined the crystallinity of PLA under different extruder temperatures, which play a vital role in enhancing mechanical properties. The results indicated that the temperature profile is directly proportional to the percentage of material crystallinity [22].

Kumar et al. evaluated the impact of 3D-PP of FFF, including levels of printing rates (30, 60 & 90 mm/sec), infill patterns (Rectangular, Triangular & Honeycomb), and layering techniques on the 3D printed multi-material PLA/PA6-TiO_2 composites. They reported that, enhanced mechanical properties were observed at an optimal printing rate of 90 mm/sec and a rectangular pattern [23]. Akhoundi et al. employed the FFF technique to fabricate the PLA specimens and compared the effect of PS on quality of the printed component and printing time. They concluded that, the increase in PS resulted in lower product quality and less printing time [24].

This study focuses on developing multi-material composites using extruded PLA and Almond shell reinforced PLA (AmdPLA) filaments and evaluating the compressive characteristics of the resulting composite. Moreover, this study investigates the impact of 3D-Printing Parameters (3D-PP), including Printing Speed (PS), Layer Height (LH), and Printing Temperature (PT) on the compressive properties by employing the Taguchi optimization methodology with an L_{16} orthogonal array. The Analysis of Variance (ANOVA) is used to identify the significant 3D-PP affecting the experimental outcome. The Signal-to-Noise (S/N) analysis helps to determine the optimal combinations of 3D-PP based on compressive strength

of the developed multi-material composite. Additionally, regression models derived from experimental outcomes are utilized to predict performance at optimal 3D-PP levels. Finally, PLA/AmdPLA is fabricated using these optimal 3D-PP to evaluate the compressive response under constant loading conditions, providing a method for developing functionally graded polymeric materials with higher load bearing capabilities.

2. Materials and Method

2.1 Raw Materials

The PLA pellets required for the filament extrusion process (specifically, INGEO 3D850) were sourced from Natur Tec Limited in the United States. These PLA granules have a white appearance and a density of 1.24 g/cm^3. Additionally, waste almond shells were obtained from the dry fruit processing industry to create Almond Shell Particles (ASP).

2.2 Preparation of ASP

After obtaining waste almond shells, they were meticulously cleaned to remove any impurities from their surfaces. Subsequently, the cleaned almond shells underwent a 12-hour drying process in a furnace at 70°C to eliminate residual moisture from the cleaning phase. Once dried, the almond shells were crushed into smaller pieces using a jaw crusher and further refined by meshing with a willy mill to achieve a uniform particle size. This meshing process was repeated until the ASP reached a consistent size. The resulting ASP was carefully filtered using a sieve shaker, resulting in ASP particles smaller than 50 μm.

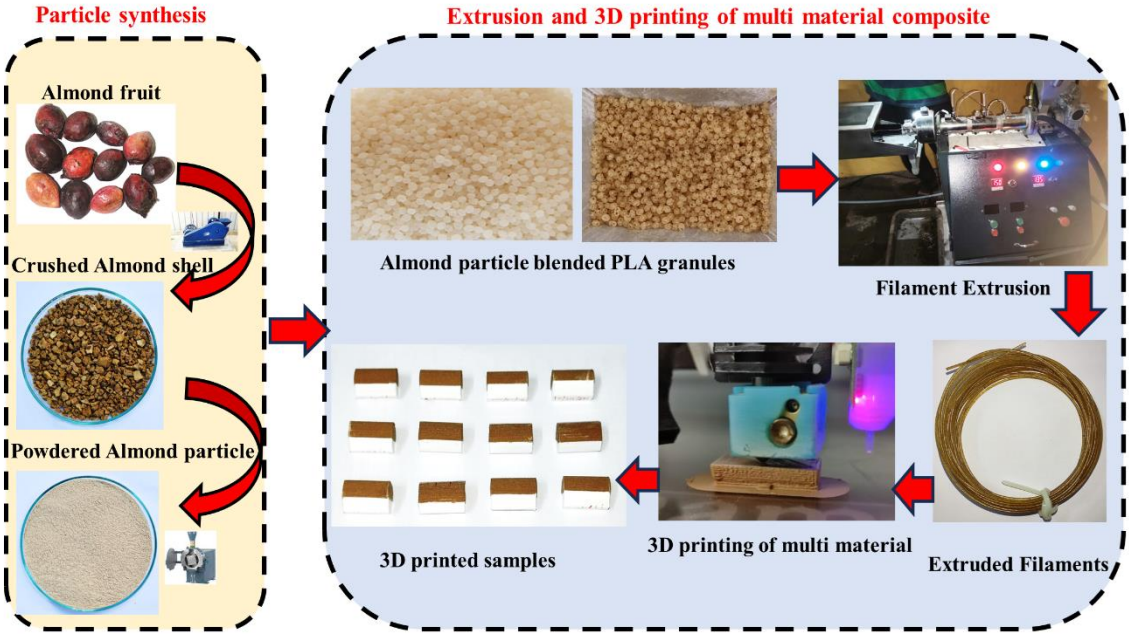

Figure 1. Schematic layout of almond shell particle synthesis and 3D printing of multi-material PLA/AmdPLA composite.

To improve the bonding between the matrix and reinforcement phases, the synthesized ASP underwent a chemical treatment with silane (Tri vinyl ethoxy silane) obtained from Sigma Aldrich in the UK. These chemically-treated ASP particles were used in the extrusion of ASP Reinforced PLA (AmdPLA) bio-composite filament. Figure 1 illustrates the process of synthesizing ASP from waste almond shells.

Table 1 Chemical composition of almond shell particle.

Raw material	Cellulose (%)	Hemicellulose (%)	Lignin (%)	Extractives (%)	Other elements (%)
Almond shell particle	37.47	27.82	30.54	-	4.17

The chemical composition of the extracted almond shell particle is shown in Table 1. The extracted particle which shows higher percentage of cellulose and which directly influences the strength of the composite. Figure 2 shows the morphology, and size distribution of the ASP particles.

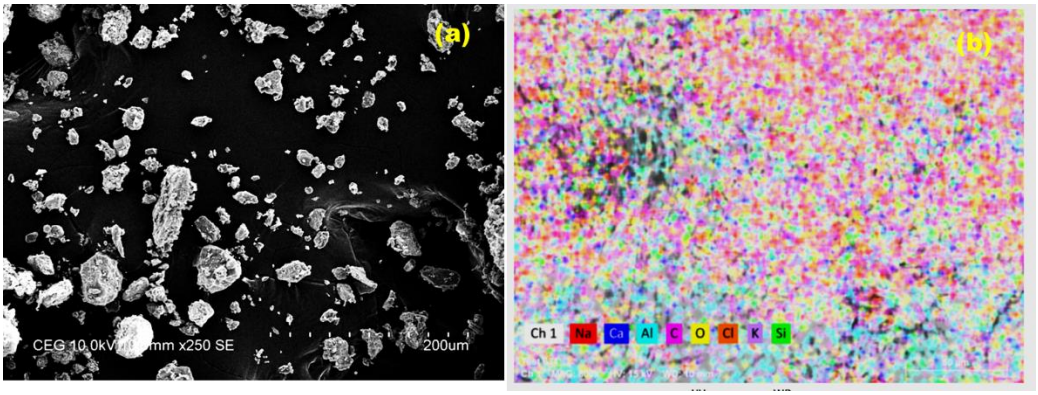

Figure 2 Morphology of ASP particle (a) SEM image, (b) EDS mapping.

The results clearly show that, the particles which are granular like spherical in shape and which are in the particle size range of 30-50 µm. From the EDS analysis, the oxygen and carbon composition of the respective ASP particles are measured. The report shows that, the carbon content of the almond shell particle would be 55.21 and oxygen content of 40.31. The oxygen to carbon (O/C) ratio of 0.73 is an indication of the added almond shell particle which are rich in cellulose and capable to adhere load and used as a reinforcement in polymer composite preparation.

2.3 Extrusion of Neat PLA and AmdPLA 3D Printing Filaments

A desktop-style filament extruder with a single screw was utilized to extrude both neat PLA and AmdPLA bio-composite filaments. Initially, neat PLA filaments were extruded within a temperature range of 135°C in the feeding zone and 150°C in the extrusion zone. Moreover, the extrusion of neat PLA filaments was carried out at an extrusion rate of 220 rpm. Additionally, the AmdPLA bio-composite filaments were extruded, comprising 90% neat PLA granules and 10% ASP.

To ensure the uniform distribution of ASP within the PLA matrix, a two-level extrusion process was employed. In the first level, the mixing chamber thoroughly combined 90% neat PLA granules and 10% ASP, and the resulting composite mixture was used for filament extrusion. The initially extruded composite filaments were then sliced into 10 mm sections during the melt-blending process. These sliced filament pieces were repeatedly fed into the hopper, and the process was repeated until the reinforcements were uniformly distributed within the polymeric PLA matrix. The extruded filaments achieved a consistent diameter of 1.75 mm ± 0.05 mm under optimized conditions. These extruded composite AmdPLA and neat PLA filaments were used as feedstock for the Fused Filament Fabrication (FFF)-based printer (Make: Pratham 2.0, India).

2.4 Development of Functionally Graded PLA/AmdPLA Material

The extruded neat PLA and AmdPLA composite filaments were used as the feedstock material for fabricating functionally graded PLA/AmdPLA materials using a FFF printer. The compression specimens were fabricated in the horizontal direction, as shown in Figure 1. For this study, the compression specimens had dimensions of 12.7 mm in diameter and 25.4 mm in height, and they were fabricated using the extruded filaments. Initially, the Computer-Aided Design (CAD) model of the specimen was created using CATIA V5R20 (Dassault Systems). The designed CAD model is then converted into a Stereolithography (STL) file. The resulting STL file is exported and imported into open-source slicers (Ultimaker Cura). The STL file was sliced according to the input 3D-PP, and the respective Geometric codes (G-codes) were generated. These G-codes were exported to a storage device, which was then used as an input for the FFF 3D printer. Figure 3 shows the 3D printed compression test samples of neat PLA/AmdPLA multi-material composites.

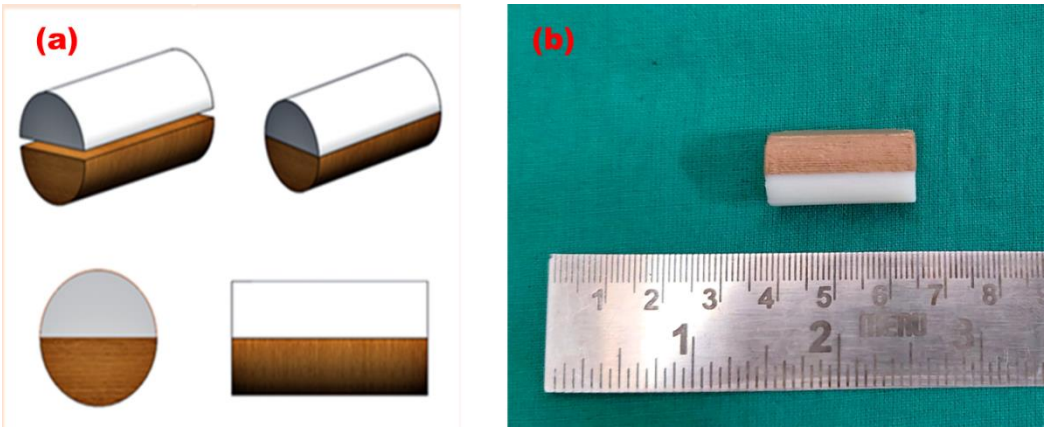

Figure 3 3D printed compression test samples of neat PLA/AmdPLA multi-material composites.

To create the functionally graded material, the number of layers was calculated using the slicing software. The calculated layer count was divided equally into two halves, with the first half consisting of layers made from neat PLA and the second half from AmdPLA composite material. For example, if 30 layers were generated for a specific set of 3D-PP, then the first 15 layers were made from neat PLA, and the subsequent 15 layers were made from AmdPLA composite material. The change of feedstock material took place after the 15th layer by pausing the FFF 3D printer. During the development of functionally graded PLA/AmdPLA material, a specific combination of 3D-PP and their respective levels were maintained at constant limits.

2.5 Mechanical Testing of prepared sample

In compression tests, the 3D printed specimens were axially compressed to measure the peak compressive strength of the PLA/AmdPLA multi-material composite. The Universal Testing Machine (UTM), along with compression test attachments, was used to conduct the compression test at a constant testing feed rate of 1 mm/min. The experiment was conducted according to the ASTM D 695 standard for compression testing. CATIA V5R20 software was employed to design the samples used in the compression test. The compression tests were executed for 3D printed PLA/AmdPLA multi-material composites along with various 3D-PP of the FFF technique. Then, the prepared specimens were placed in the machine axially, and load was applied.

2.6 Selection and optimization of 3D-PP

Table.2 3D-PP and levels for the FFF process.

Sl. No.	3D-PP	Unit	Level

			1	2	3	4
1	Printing Speed (PS)	mm/sec	10	20	30	40
2	Layer Height (LH)	mm	0.1	0.15	0.2	0.25
3	Printing Temperature (PT)	℃	190	200	210	220

In this study, three different 3D-PP, namely PS, LH, and PT, were varied and optimized to develop effective samples of 3D printed PLA/AmdPLA multi-material composite. Three 3D-PP and four levels were selected to run the experiments, and Design of Experiments (DOE) was used to label the experimental runs. The various levels and 3D-PP are shown in Table 2, which can be used to determine the optimal conditions of the 3D printing process.

The L_{16} Taguchi orthogonal array was chosen to carry out the experimental runs of the 3D printing process, as the study considered three factors and four levels. Five samples were tested for each set of 3D-PP to analyze the predicted and experimental error. Using Minitab 2020 software, the influential factors and interaction effects were examined. Experimental runs were selected for the optimization process based on a p-value of less than 0.05. Additionally, the independent variables (PS, LH, and PT) and the dependent variable (compressive strength) were employed to forecast the regression equation and model for an optimal fit.

The "larger the best" condition was chosen to optimize the compressive strength of the PLA/AmdPLA specimen. The equation for the corresponding response is illustrated below.

$$\frac{S}{N} = -10 * log_{10}(\frac{1}{y^2}) \quad (1)$$

Where 'Y' represents the response of the FFF printed PLA/AmdPLA multi-material polymeric composite, such as compressive strength.

2.7 Characterization of compressive tested polymeric sample

Stereo microscopic observations are conducted to investigate the surface characteristics and failure modes of PLA/AmdPLA multi-material composite compressive samples. The impact of 3D-PP on layer interface adhesion and print quality is evaluated using microscopic observation. After failure, samples are used to investigate the failure modes, crushing patterns, and interlayer failures of the tested compressive 3D printed PLA/AmdPLA multi-material compressive samples.

3. Results and Discussion

The various 3D-PP, such as PS (10, 20, 30, and 40 mm/s), LH (0.1, 0.15, 0.2, and 0.25 mm), and PT (190°C, 200°C, 210°C, and 220°C), were used to print the 16 different sets of multi-material samples, and compressive strength was analyzed on those samples. The obtained

compressive strength results are listed in Table 3. The compressive strength was taken into consideration, and the effects of each 3D-PP and the most effective combinations were examined in the sections below.

Table 3. L_{16} array and its results for the compressive test experiments.

Sl. No.	PS (mm/s)	LH (mm)	PT (°C)	Compressive strength (MPa)
1	10	0.1	190	27.44
2	10	0.15	200	26.29
3	10	0.2	210	25.03
4	10	0.25	220	21.35
5	20	0.1	200	35.41
6	20	0.15	190	26.69
7	20	0.2	220	32.21
8	20	0.25	210	29.24
9	30	0.1	210	31.01
10	30	0.15	220	25.08
11	30	0.2	190	19.54
12	30	0.25	200	20.05
13	40	0.1	220	24.87
14	40	0.15	210	20.24
15	40	0.2	200	16.24
16	40	0.25	190	13.27

3.1 Statistical Analysis of compressive strength of the PLA/ AmdPLA multi-material composites

This section investigates the primary consequences of 3D-PP on the compressive strength of the developed PLA/AmdPLA multi-material composites. The mean of the Signal to Noise (SN) ratios for the compressive strength responses is presented in Figure 4 with respect to each 3D-PP, including PS, LH, and PT. Figure 4 indicates the compressive strength characteristics of PLA/AmdPLA multi-material composites, which are significantly influenced by various 3D-PP.

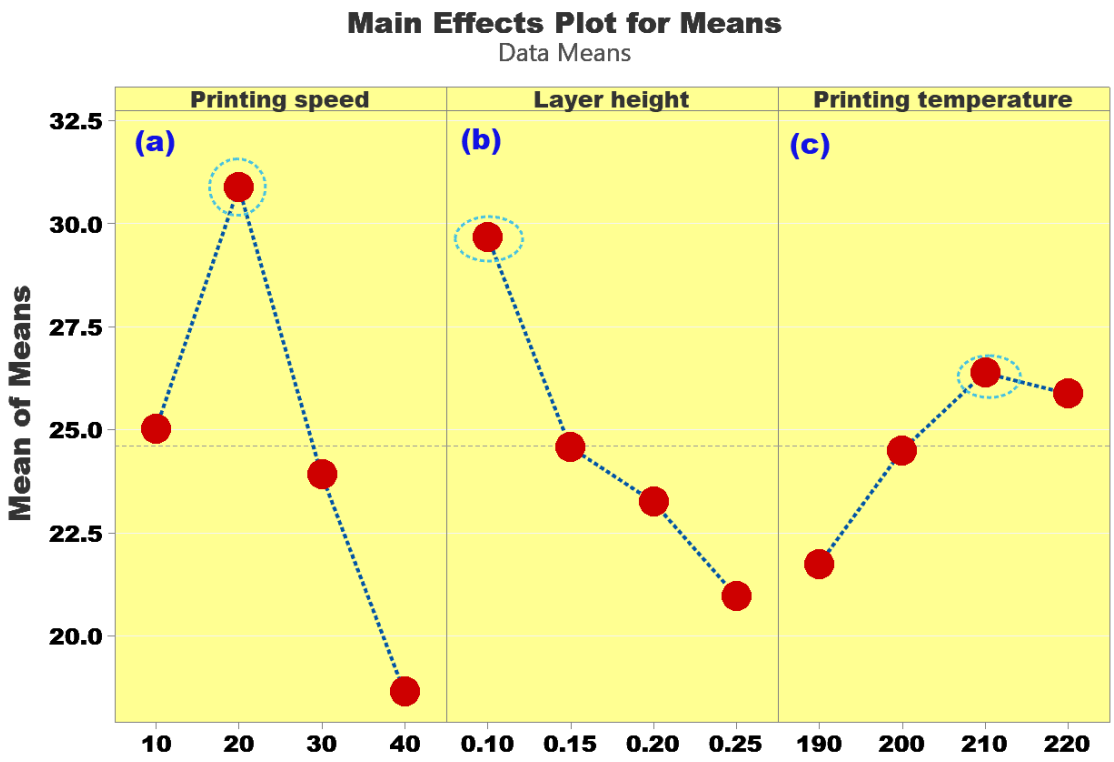

Figure 4. SN plot for the compressive strength of 3D printed PLA/AmdPLA multi-material composites.

The most significant impact plot of printing PLA/AmdPLA multi-material composites with different 3D-PP, such as PS with variable levels of 10, 20, 30, and 40 mm/s, is shown in Figure 4 (a). According to the findings, printing at a speed of 20 mm/s produced a maximum compressive strength of 29.24 MPa. The compressive strength starts to decline after 20 mm/s. Considering the multi-material composites, the interaction of two different materials mainly occurred at the interface. For the current case, the material deposition at higher speeds does not allow enough time for proper sequential material deposition, resulting in weak interfacial adhesion between the deposited PLA and AmdPLA zones. Insufficient heating and cooling can result in incomplete fusion among the deposited polymeric composite layers, leading to weakened inter-layer adhesion. This occurs because there is not enough time for a solid bond to form between the PLA and AmdPLA layers [25]. The improper material deposition results in the development of voids along the interface of the printed structure. These voids contribute to an increase in porosity, resulting in a reduced overall density of the printed object. Consequently, this compromised fusion and increased porosity lead to a decline in the compressive strength of the printed object. Hence, higher PSs have an adverse impact on the quality, density, and structural integrity of the printed part [26]. Therefore, the lowest compressive strength of 25 MPa is revealed by the faster PS of 40 mm/s. Similar studies were

reported by Veeman et al. on wood/PLA composites regarding the evaluation of compressive strength performance under higher PS conditions [27].

Figure 4 (b) illustrates the influence of various LH values, such as 0.10, 0.15, 0.20, and 0.25 mm, on the compressive strength of the PLA/AmdPLA multi-material composites. It is evident that the compressive strength of the composites continuously declined as the LH was increased. The least compressive strength was obtained at the highest LH of 0.25 mm. In contrast, when the LH was reduced to 0.10 mm, the compressive strength increased significantly to 29.5 MPa. This is because at lower LH, the width of each layer was lower and could melt the PLA effectively and fuse easily with the adjacent AmdPLA layers. Employing a lower LH in the 3D printing of multi-material composite materials allows for printing a greater number of layers. Thinner layers exhibit improved layer adhesion, resulting in better bonding between individual layers of material. Thinner layers offer a larger surface area for the material to adhere to, facilitating a stronger bond between the layers, which is favourable for the material's compressive properties [28]. Increasing the LH during 3D printing can contribute to the creation of voids and gaps between layers. When thicker layers are printed, the material may not flow and distribute evenly, leading to incomplete filling of the gaps between adjacent layers. As a consequence, empty spaces or voids can form within the printed object, significantly affecting its structural integrity. These voids act as areas of weakness and can concentrate stresses, potentially reducing the compressive strength of the object [29]. Kuznetsov et al. reported a similar conclusion regarding the LH response on 3D printed polymer composite samples [30].

Figure 4 (c) illustrates the relationship between the compressive strength of PLA/AmdPLA multi-material composites and different PTs, namely 190°C, 200°C, 210°C, and 220°C. The compressive strength of the composites exhibits a significant increase up to 210°C. This can be attributed to the decrease in viscosity of the PLA composites as the temperature rises. The lower viscosity facilitates enhanced fusion between the polymer layers, resulting in improved interlayer bonding and reduced porosity within the printed object, thereby substantially enhancing the compressive strength of the PLA composite material [31]. However, beyond 210°C, the compressive strength starts to decrease. This decline can be attributed to the increase in the chance of over-melting of the polymeric material and effectively results in the development of crest and troughs in the deposited layers. These alterations adversely affect the material's mechanical properties, including compressive strength, leading to a decrease in overall strength. Therefore, maintaining the PT within the optimal range, particularly around 210°C, is crucial for achieving maximum compressive

strength in PLA composite materials [32]. According to the overall findings, the maximum compressive strength of PLA/AmdPLA multi-material composites was reported at a printing speed of 20 mm/sec, an LH of 0.1 mm, and a PT of 210°C.

Table 4. Response table for the various 3D-PP regarding compressive strength.

Level	PS (mm/s)	LH (mm)	PT (°C)
1	25.03	29.68	21.73
2	30.89	24.57	24.50
3	23.92	23.25	26.38
4	18.65	20.98	25.88
Delta	12.23	8.71	4.64
Rank	1	2	3

From the average of the SN values of each 3D-PP and levels, the delta value is measured, and the ranking is based on the observed delta value. Based on the respective findings, the order of influencing factors for PLA/AmdPLA multi-material composites was investigated. The response table for the SN for the compressive strength property of the composite made from 3D printed PLA/AmdPLA composites is shown in Table 4. The most important 3D-PP and the order of the influential 3D-PP sequence of the respective compressive strength property of the PLA/AmdPLA multi-material composite produced by 3D printing was PS, LH, and PT. The compressive strength characteristic of the PLA/AmdPLA multi-material composites is significantly impacted by PS, as compared with other 3D-PP.

3.2. Analysis of Variance and Regression analysis of the compressive strength analysis

The section aims to investigate the individual interaction and contribution of each 3D-PP in the compressive experiments on the 3D printed PLA/AmdPLA multi-material composites. The ANOVA test was conducted to analyze the percentage contribution of each factor, including PS, LH, and PT, with respect to the compressive strength. Table 5 displays the ANOVA results, highlighting the significance of each factor on the compressive strength of the 3D printed PLA/AmdPLA multi-material composites.

Table 5. ANOVA results for compressive strength of the PLA/AmdPLA multi-material composites.

Source	DF	Adj SS	Adj MS	F-Value	P-Value	Percentage contribution

PS (mm/sec)	3	302.08	100.692	59.81	0.000	57.29
LH (mm)	3	163.05	54.349	32.28	0.000	30.92
PT (°C)	3	52.07	17.356	10.31	0.009	9.87
Error	6	10.10	1.684			1.92
Total	15	527.29				100

In the optimization experiments, a P-value below 0.05 was considered significant. If the P-value exceeded this threshold value, it indicated that the respective factor was insignificant, implying that the particular 3D-PP did not have a notable influence on the compressive strength of the PLA/AmdPLA multi-material composites. Based on the observed results presented in Table 4, the PS, LH, and PT exhibited P-values below 0.05, indicating their significant effects on the compressive strength.

Therefore, the findings suggest that careful consideration and optimization of the PS, LH, and PT are crucial in order to achieve desired levels of compressive strength in the PLA/AmdPLA multi-material composites. These 3D-PP play important roles in determining the overall mechanical properties of the 3D printed composite material.

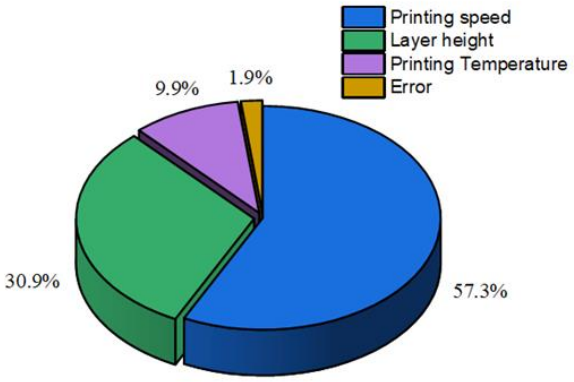

Figure 5. Percentage contribution plot of 3D-PP for the PLA/AmdPLA multi-material composites.

Figure 5 illustrates the percentage contribution plot of the 3D printing process in relation to the compressive properties of the newly fabricated PLA/AmdPLA multi-material composites. The analysis reveals that the PS accounts for the largest contribution, amounting to 59.29%. Following closely, the LH demonstrates a significant contribution of 30.92%. Conversely, the PT exhibits a comparatively smaller contribution of 9.87%.

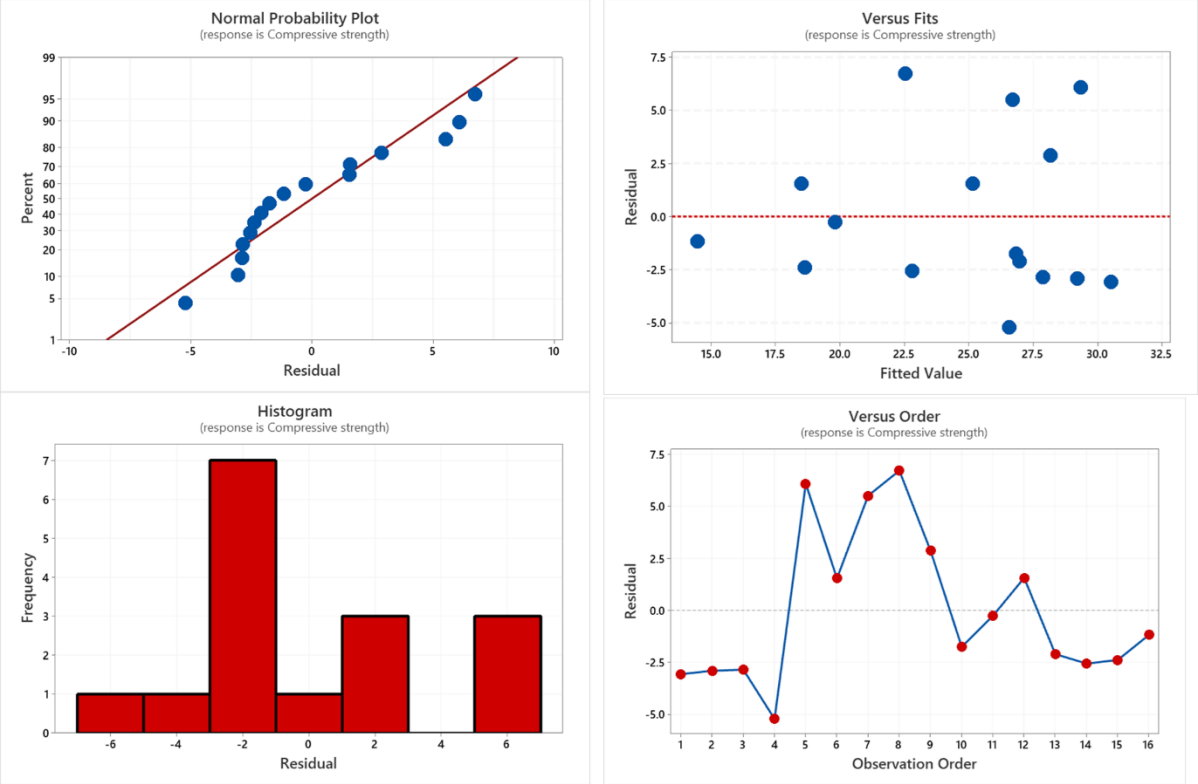

Figure 6. Residual plot for compressive strength of PLA/AmdPLA multi-material composites.

The residual plot for the compressive strength of the PLA/AmdPLA multi-material composites is presented in Figure 6. By using the regression equation (2), for the optimized condition, the compressive strength of the multi-material was measured. The plot demonstrates that all the data points align with the normal line in the probability plot. This indicates that the prediction model accurately captures the behavior of the composite material, and the model fit is deemed satisfactory.

$$Compressive\ strength = 11.4 - 0.2609\ Printing\ speed - 54.9\ Layer\ height + 0.1431\ Printing\ Temperature \quad (2)$$

The results of the compression test experiments are presented in Table 6, showcasing the optimal combination outcomes for both the experimental and predicted conditions. Upon conducting the tests on the optimal combination of 3D-PP of the PLA/AmdPLA multi-material composites, compressive strengths of 32.247 and 33.743 MPa were recorded, both in the experimental and predicted scenarios. The error percentage for the predicted mathematical model is 4.63%, which falls within the acceptable range. This indicates that the predicted model provides a reasonably accurate estimation of the compressive strength for the PLA/AmdPLA multi-material composites.

Table 6. Confirmation experiments and its error percentage for the predicted model.

Response	Optimal levels of 3D-PP	Predicted value	Experimental value	Percentage error (%)
Compressive strength (MPa)	PS (mm/sec) – 20 LH (mm) – 0.1 PT (°C) - 210	33.743	32.247	4.63

The PLA/AmdPLA multi-material composites samples are 3D printed at the optimised levels of 3D-PPs. The optimized condition samples are tested under compressive load, and the optimal stress value was determined. The experimental results show that the experimental value of 32.24 MPa was observed on the PLA/AmdPLA multi-material composites as depicted in Figure 7. And the fractured samples undergo bulging mode of failure. This implies the samples uphold the maximum and transfer the stress before failure which evidently resulted in higher strain rates. Moreover, the PLA specimens fabricated at the same level of printing parameters resulted in slightly lower compressive strength of 30.59 Mpa and developed fractures at the earlier stage in comparison to the multi-material specimens. In addition, the AmdPLA composite attained a higher compressive strength of 36.73 Mpa within a moderate load-bearing capacity.

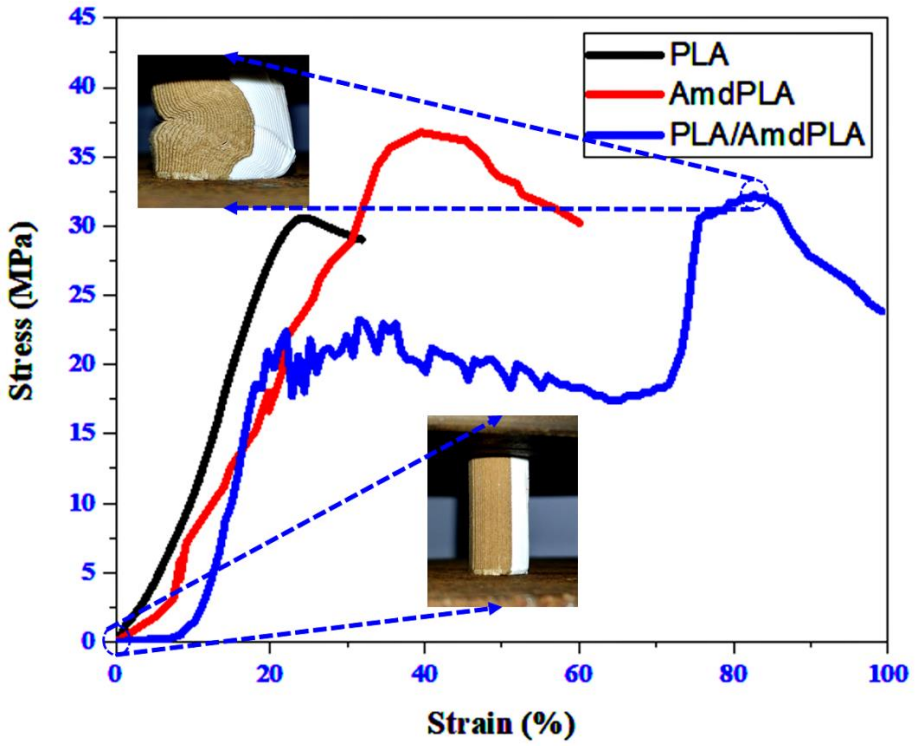

Figure 7. Optimal stress strain curves of PLA, AmdPLA, and PLA/AmdPLA specimens

3.3. Surface characterization of the PLA/AmdPLA multi-material printed composite

Surface characterization of the 3D printed PLA/AmdPLA multi-material composites was analyzed through Stereo microscopic technique. Figure 8 shows the stereo images of the PLA/AmdPLA multi-material composites with respect to the LH. Figure 8 (a-c) show the impact of LH on the development of this particular multi-material composites. These figures clearly show that at lower LH, the number of layers is higher and the compatibility was good at the interface.

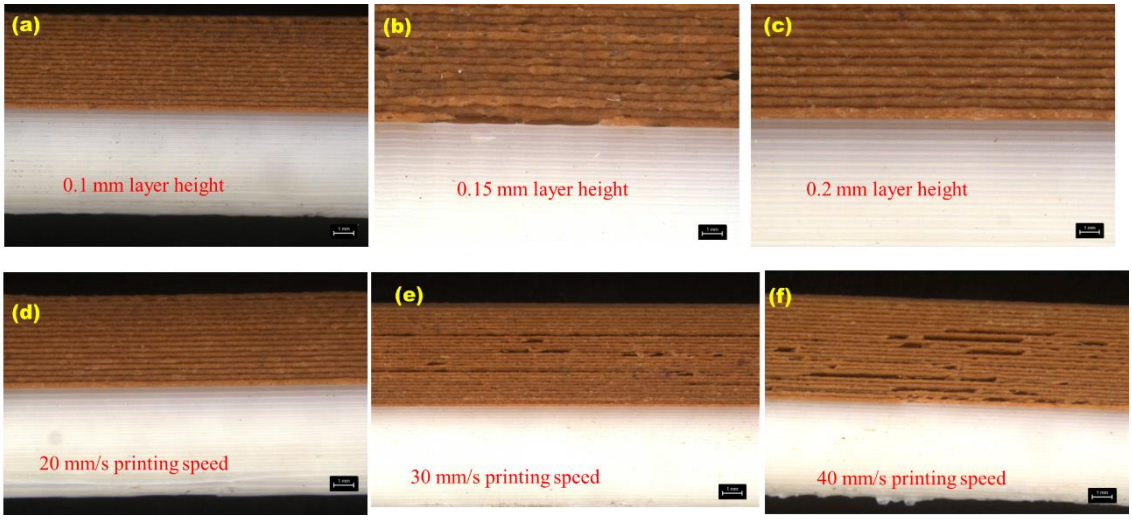

Figure 8. Stereo microscopic images of 3D printed PLA/AmdPLA multi-material.

In the case of considering the higher LHs such as 0.15mm and 0.20mm, at the interface there is a presence of interfacial gaps and voids. This may act as a failure-initiating zone during the compression test. Figure 8 (d-f) shows the impact of PS on the development of PLA/AmdPLA multi-material composites. From the observed images, beyond 20mm/s of PS, there is an observance of layer peel-off at the interface. Increases in the PS may impact the reduction in the compressive strength. This is based on the insufficient material deposition and presence of large voids in both the interface and the composite materials.

3.4. Fractographical analysis of the fractured samples

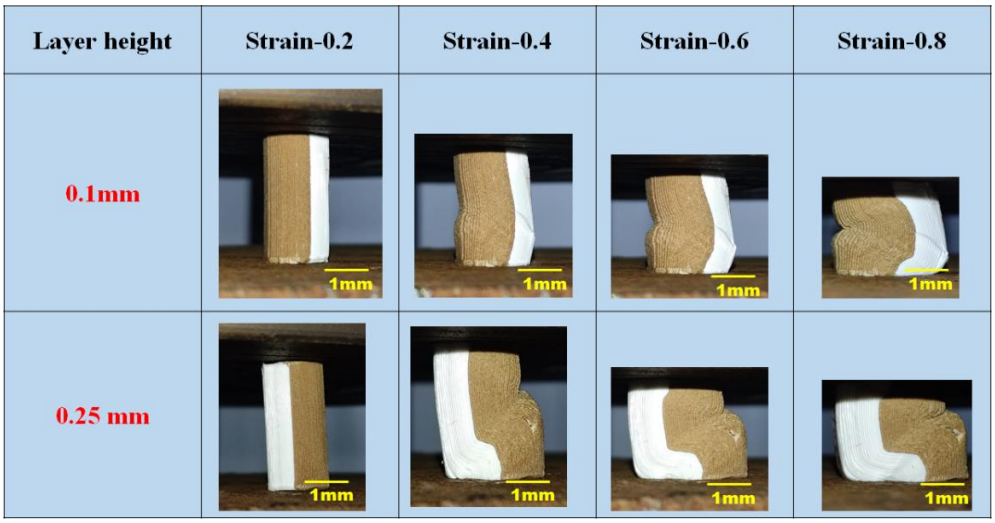

Figure 9. Fractographical analysis of 3D printed PLA/AmdPLA material with respect to LH.

Figure 9 shows the mode of fractures occurred during the compression test of the developed PLA/AmdPLA multi-material composites under various strain rates. From the obtained results, the impact of LH was sequentially observed with respect to varying the strain rate. At lower LH of 0.1mm, it exhibits bulging, and there is no layer peel-off until it reaches the 0.6mm of strain rate. This may imply the layer adhesion was good, and the fracture occurred under bulging mode. In the case of considering the 0.25mm of LH, the samples failed under buckling, and the samples may bend and slide. Among the results, the AmdPLA portion exhibits higher flexibility when compared to PLA matrix zone.

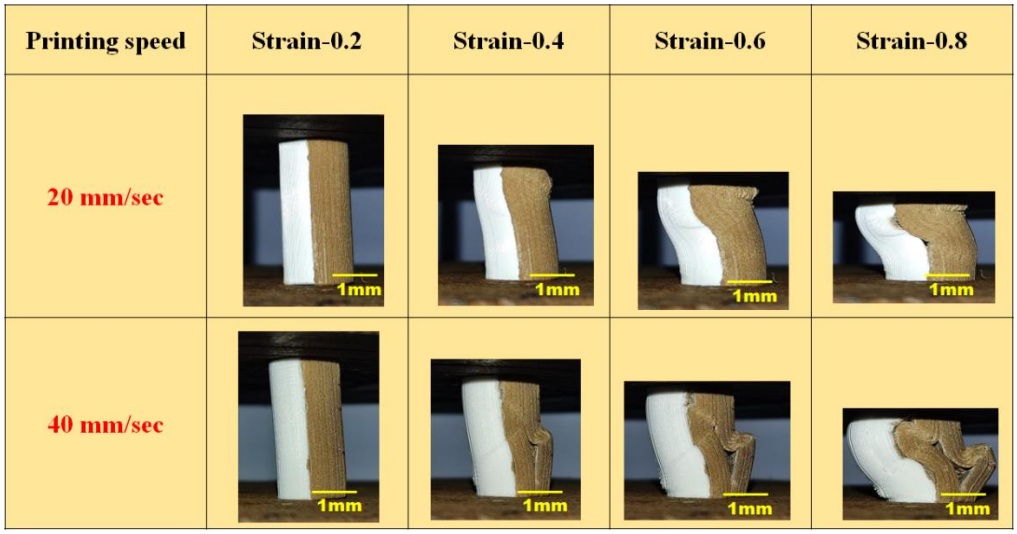

Figure 10. Fractographical analysis of 3D printed PLA/AmdPLA material with respect to PS.

Figure 10 shows the mode of fractures occurred during the compression test of the developed PLA/AmdPLA multi-material composites under various strain rates with respect to PS. Considering the print speed, the samples printed at 20 mm/sec show higher compressive strength, and the samples fail under bulging mode. During the compression test, at the failure point, layer peel-off occurred at the interface. This indicates that the samples may withstand minimal load and fail at the interface. In the case of considering a higher PS of 40 mm/sec, the sample layers peel off at both the interface and the AmdPLA portion. This is due to the added ASP layers generating voids at the interface, reducing the interfacial adhesion between adjacent layers. This void formation is clearly evidenced from Figure 8(f), and the layers are delaminated under compressive load with respect to higher PS condition printed samples.

3.5. Application and Surface feature analysis of compression tested multi material samples:

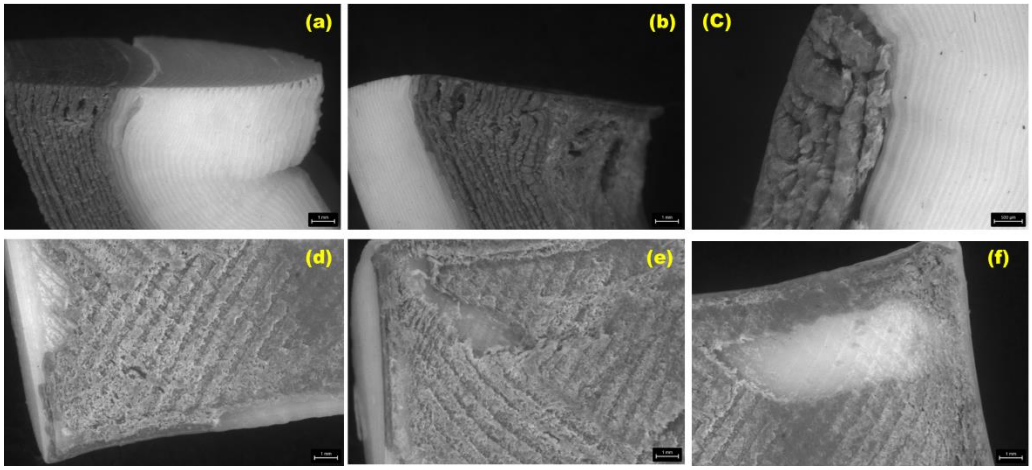

Figure 11 Microscopic images of the fractured PLA/AmdPLA multi-material composites (a) layer height of 0.1, (b) layer height of 0.2, (c) layer height of 0.25, (d) printing speed of 10mm/sec (e) printing speed of 20mm/sec and (f) printing speed of 30mm/sec.

Figure 11 shows the microscopic images of the fractured PLA/AmdPLA multi-material composites. Figure 11 (a-c) shows the impact of layer height on the compressive fractured samples. Under compressive loading the samples layers are detached and starts to fail. In case of lower layer height, the sample layer detachment was less compared to higher layer height samples. Considering the multi material composites, overall, in the AmdPLA side the layer detachment was higher compared to PLA side. Figure 11 (d-f) shows the impact of printing speed on the compressive fractured samples. The results show that, at lower printing speed of 10mm/sec, there is an over material extrusion and there is an observation of edge detachment at the boundaries of the interface. In case of printing speed of 20mm/sec, there is no layer

detachment at the interface and the detachment occurred at the interfacial layers of the AmdPLA side. Considering higher printing speed of 30mm/sec there is an higher volume of layer detachment due to improper bonding at the interfaces of two different materials.

The PLA/AmdPLA multi-material composites are gaining popularity across various consumer goods due to their blend of sustainability, aesthetic appeal, and functionality. These functional materials are ideal for creating products that require both light-weighting and durability characteristics like window casings, decorative pieces and facades. Moreover, the natural, wood-like appearance of these multi-material composites is highly valued for its aesthetic appeal and they can be fabricated into any intricate designs, offering a unique blend of natural beauty and modern manufacturing capabilities. In addition, they materials are highly effective in architectural prototyping due to their realistic appearance, versatility, and durability. They enable the creation of detailed and visually appealing scale models, enhancing the accuracy and aesthetic appeal of architectural representations. Overall, these multi-material composites are known for their enhanced strength, light-weighing, aesthetic appeal and sustainability across a wide range of consumer applications.

4. Conclusions

After conducting the optimization study on the developed PLA/AmdPLA multi-material composites, the optimal combination of 3D-PP for fabricating compression samples has been found as a PS of 20 mm/sec, a LH of 0.1 mm, and a PT of 210°C. These specific 3D-PP settings have been identified as the most favourable for achieving the desired quality and properties in the fabrication process of the PLA/AmdPLA multi-material composite. The influential factors and their order of importance in the 3D printing process of the PLA/AmdPLA multi-material composite have been determined to be PS as the most influential, followed by LH, and then PT. This indicates that adjusting the PS has the greatest impact on the final properties of the printed composite, followed by fine-tuning the LH and PT. Based on the regression analysis results, the compression tests conducted on the PLA/Wood multi-material composite exhibited an error percentage of 4.73%. This indicates that the predicted values from the regression model closely align with the experimental results, demonstrating a high level of accuracy. So, these functional composite materials are recognized for their superior strength, lightweight properties, attractive appearance, and sustainability in various consumer applications.

Acknowledgment:

The authors acknowledge the Researchers Supporting Project number (RSPD2023R674), King Saud University, Riyadh, Saudi Arabia for funding this research work.

Data Availability statement:

The data that support the findings of this study are available from the corresponding author, upon reasonable request.

References

1. Zhang, Chi, Fei Chen, Zhifeng Huang, Mingyong Jia, Guiyi Chen, Yongqiang Ye, Yaojun Lin et al. "Additive manufacturing of functionally graded materials: A review." Materials Science and Engineering: A 764 (2019): 138209.
2. Brenken, Bastian, Eduardo Barocio, Anthony Favaloro, Vlastimil Kunc, and R. Byron Pipes. "Fused filament fabrication of fiber-reinforced polymers: A review." Additive Manufacturing 21 (2018): 1-16.
3. Sivakumar, Narain Kumar, Sabarinathan Palaniyappan, Santhosh Basavarajappa, Mohamed Ibrahim Hashem, Mahdi Bodaghi, and Vignesh Sekar. "Study on the impact of material extrusion factors on the compressive characteristics of honeycomb lattice-structured Onyx™ composites." Materials Today Communications 37 (2023): 107317.
4. Kumar, Sudhir, Rupinder Singh, T. P. Singh, and Ajay Batish. "Fused filament fabrication: A comprehensive review." Journal of Thermoplastic Composite Materials 36, no. 2 (2023): 794-814.
5. Yang, Nuo, Shiqian Hu, Dengke Ma, Tingyu Lu, and Baowen Li. "Nanoscale graphene disk: a natural functionally graded material–how is Fourier's law violated along radius direction of 2D disk." Scientific reports 5, no. 1 (2015): 14878.
6. Zhang, Binbin, Prakhar Jaiswal, Rahul Rai, and Saigopal Nelaturi. "Additive manufacturing of functionally graded material objects: a review." Journal of Computing and Information Science in Engineering 18, no. 4 (2018): 041002.
7. Kawasaki, Akira, and Ryuzo Watanabe. "Concept and P/M fabrication of functionally gradient materials." Ceramics international 23, no. 1 (1997): 73-83.
8. Kumar, Suresh, KVVS Murthy Reddy, Anil Kumar, and G. Rohini Devi. "Development and characterization of polymer–ceramic continuous fiber reinforced functionally graded composites for aerospace application." Aerospace Science and Technology 26, no. 1 (2013): 185-191.
9. Du, Dafan, Yves Fautrelle, Anping Dong, Da Shu, Guoliang Zhu, Baode Sun, Henri Nguyen-Thi, Zhongming Ren, and Xi Li. "In-situ fabrication of graded material with the application of a horizontal magnetic field during directional solidification." Materials Characterization 141 (2018): 423-432.
10. Loh, Giselle Hsiang, Eujin Pei, David Harrison, and Mario D. Monzón. "An overview of functionally graded additive manufacturing." Additive Manufacturing 23 (2018): 34-44.

11. Tofail, Syed AM, Elias P. Koumoulos, Amit Bandyopadhyay, Susmita Bose, Lisa O'Donoghue, and Costas Charitidis. "Additive manufacturing: scientific and technological challenges, market uptake and opportunities." Materials today 21, no. 1 (2018): 22-37.

12. Singh, R., Kumar, R., Farina, I., Colangelo, F., Feo, L., & Fraternali, F. (2019). Multi-material additive manufacturing of sustainable innovative materials and structures. Polymers, 11(1), 62.

13. Baca Lopez, D. M., & Ahmad, R. (2020). Tensile mechanical behaviour of multi-polymer sandwich structures via fused deposition modelling. Polymers, 12(3), 651.

14. Cojocaru, V., Frunzaverde, D., Miclosina, C. O., & Marginean, G. (2022). The influence of the process parameters on the mechanical properties of PLA specimens produced by fused filament fabrication—A review. Polymers, 14(5), 886.

15. Akhoundi, B., Behravesh, A. H., & Bagheri Saed, A. (2020). An innovative design approach in three-dimensional printing of continuous fiber–reinforced thermoplastic composites via fused deposition modeling process: in-melt simultaneous impregnation. Proceedings of the Institution of Mechanical Engineers, Part B: Journal of Engineering Manufacture, 234(1-2), 243-259.

16. Li, Rui, Anand Kumar Sharma, Junchao Zhu, Bo Zheng, Gengsheng Xiao, and Ling Chen. "Nutritional biology of chestnuts: A perspective review." Food Chemistry 395 (2022): 133575.

17. Jena, D. K., & Sahoo, P. K. (2018). Simultaneous improvement of mechanical and fire retardant properties of synthesised biodegradable guar gum-g-poly (butyl acrylate)/montmorillonite nanocomposite. Polymer Degradation and Stability, 154, 37-45.

18. Huda, M. S., Drzal, L. T., Misra, M., & Mohanty, A. K. (2006). Wood-fiber-reinforced poly (lactic acid) composites: evaluation of the physicomechanical and morphological properties. Journal of applied polymer science, 102(5), 4856-4869.

19. Palaniyappan, Sabarinathan, Gnanavelbabu Annamalai, Narain kumar Sivakumar, and Prahadeeswaran Muthu. "Development of functional gradient multi-material composites using Poly Lactic Acid and walnut shell reinforced Poly Lactic Acid filaments by fused filament fabrication technology." Journal of Building Engineering 65 (2023): 105746.

20. Ayrilmis, N., Kariz, M., Kwon, J. H., & Kitek Kuzman, M. (2019). Effect of printing layer thickness on water absorption and mechanical properties of 3D-printed wood/PLA composite materials. The International Journal of Advanced Manufacturing Technology, 102, 2195-2200.

21. Chohan, J. S., Mittal, N., Kumar, R., Singh, S., Sharma, S., Singh, J., ... & Dwivedi, S. P. (2020). Mechanical strength enhancement of 3D printed acrylonitrile butadiene styrene polymer components using neural network optimization algorithm. Polymers, 12(10), 2250.

22. Vanaei, H., Shirinbayan, M., Deligant, M., Raissi, K., Fitoussi, J., Khelladi, S., & Tcharkhtchi, A. (2020). Influence of process parameters on thermal and mechanical properties of polylactic acid fabricated by fused filament fabrication. Polymer Engineering & Science, 60(8), 1822-1831.

23. Kumar, S., Singh, R., & Singh, M. (2022). Multi-material 3D printed PLA/PA6-TiO2 composite matrix: rheological, thermal, tensile, morphological and 4D capabilities. Advances in Materials and Processing Technologies, 8(2), 2329-2348.

24. Akhoundi, B., Nabipour, M., Kordi, O., & Hajami, F. (2023). Calculating printing speed in order to correctly print PLA/continuous glass fiber composites via fused filament fabrication 3D printer. Journal of Thermoplastic Composite Materials, 36(1), 162-181.

25. Abeykoon, C., Sri-Amphorn, P., & Fernando, A. (2020). Optimization of fused deposition modeling parameters for improved PLA and ABS 3D printed structures. International Journal of Lightweight Materials and Manufacture, 3(3), 284-297.

26. Dave, H. K., Rajpurohit, S. R., Patadiya, N. H., Dave, S. J., Sharma, K. S., Thambad, S. S., ... & Sheth, K. V. (2019). Compressive strength of PLA based scaffolds: effect of layer height, infill density and print speed. Int. J. Mod. Manuf. Technol, 11(1), 21-27.

27. Veeman, D., & Palaniyappan, S. (2022). Process optimisation on the compressive strength property for the 3D printing of PLA/almond shell composite. Journal of Thermoplastic Composite Materials, 08927057221092327.

28. Yu, Z., Gao, Y., Jiang, J., Gu, H., Lv, S., Ni, H., ... & Jia, C. (2019, November). Study on effects of FDM 3D printing parameters on mechanical properties of polylactic acid. In IOP Conference Series: Materials Science and Engineering (Vol. 688, No. 3, p. 033026). IOP Publishing.

29. Shubham, P., Sikidar, A., & Chand, T. (2016). The influence of layer thickness on mechanical properties of the 3D printed ABS polymer by fused deposition modeling. Key engineering materials, 706, 63-67.

30. Kuznetsov, V. E., Solonin, A. N., Urzhumtsev, O. D., Schilling, R., & Tavitov, A. G. (2018). Strength of PLA components fabricated with fused deposition technology using a desktop 3D printer as a function of geometrical parameters of the process. Polymers, 10(3), 313.

31. Hsueh, M. H., Lai, C. J., Wang, S. H., Zeng, Y. S., Hsieh, C. H., Pan, C. Y., & Huang, W. C. (2021). Effect of printing parameters on the thermal and mechanical properties of 3d-printed pla and petg, using fused deposition modeling. Polymers, 13(11), 1758.

32. Frunzaverde, D., Cojocaru, V., Ciubotariu, C. R., Miclosina, C. O., Ardeljan, D. D., Ignat, E. F., & Marginean, G. (2022). The influence of the printing temperature and the filament color on the dimensional accuracy, tensile strength, and friction performance of FFF-printed PLA specimens. Polymers, 14(10), 1978.